



Cite this: *CrystEngComm*, 2026, 28, 577

When halogen bonding isn't enough: solvation behavior in ionic cocrystals of benzyltrimethylammonium halides and 1,4-diiodotetrafluorobenzene†

Andrew J. Peloquin,^a Lahiruni Pelendage,^a Srikar Alapati,^b Timothy W. Hanks,^b Colin D. McMillen^{*a} and William T. Pennington^{id}^{*a}

The role of halide anion identity and the influence of reaction solvent on the resulting halogen-bonded assembly was explored by combining 1,4-diiodo-tetrafluorobenzene (*p*-F₄DIB) with trimethylbenzyl ammonium halides (NMe₃BzX, X = Cl, Br, I) in diverse organic solvents. Iodide salts predominantly yielded solvated crystalline products when the salt cocrystallized in an equimolar ratio with *p*-F₄DIB. In solvent systems where the iodides did not crystallize as solvates, the salt:organoiodine ionic cocrystal ratio departed from the 1:1 reaction stoichiometry, producing 8:3, 4:5, or 2:3 cocrystals. In contrast, bromide and chloride analogues favored unsolvated forms, with chloride consistently producing a single 1:1 motif across multiple solvents. A small number of solvated forms were isolated in the Br and Cl series, typically at matched donor:acceptor ratios. Notably, chloride and bromide salts formed nearly indistinguishable halogen-bonded networks, apart from differences attributable to anion size. These results emphasize the delicate balance between solvent, stoichiometry, and halide identity in directing halogen-bond-driven crystallization.

Received 26th August 2025,
Accepted 22nd November 2025

DOI: 10.1039/d5ce00832h

rsc.li/crystengcomm

Introduction

Halogen bonding has become a central strategy in the design of supramolecular architectures, offering a directional, predictable, and highly tunable noncovalent interaction between a polarized halogen atom and an electron donor site.^{1,2} This interaction, driven by the anisotropic distribution of electron density around halogen atoms, particularly iodine and bromine, has been widely exploited to construct cocrystals,^{3–5} molecular assemblies,^{6–8} and functional materials.⁹ Halogen bonding complements and sometimes rivals hydrogen bonding in strength and selectivity, offering unique advantages in crystal engineering where geometrical precision is crucial.^{7,10,11} Halogen bonding is an essential force in supramolecular chemistry,^{10,12,13} liquid crystal formation,^{14–16} and pharmaceutical development.^{17,18}

Building on these advances, solvated halogen-bonded cocrystals—crystalline materials in which solvent molecules are incorporated into the lattice—present a compelling

subfield for exploration. Solvent molecules can participate directly in halogen bonding or indirectly modulate crystal packing *via* secondary interactions, such as hydrogen bonding, van der Waals forces, or π -stacking.^{19,20} Their presence can stabilize otherwise inaccessible packing motifs,^{21–24} resulting in diverse or tunable physical properties such as thermal behavior, mechanical integrity, and solubility.^{25,26} For example, tetrahaloethynyl resorcinarene cavitations have been studied as solvates, where the structural flexibility of the cavitation was essential to the resulting solid-state structure. The authors noted “unpredictable intermolecular interactions where the fine balance between halogen and hydrogen bonding drives the crystallization process”.²⁷ Understanding the role of solvent inclusion is particularly relevant for pharmaceutical development, where control over solvate formation and desolvation profiles is crucial for manufacturability and regulatory compliance.^{28,29} Despite their practical relevance, solvated halogen-bonded cocrystals remain relatively underexplored compared to their hydrogen-bonded counterparts, offering a fertile ground for expanding the toolkit of crystal design.

Herein, we report the isolation of twenty ionic cocrystals obtained by the reaction of the common halogen bond donor 1,4-diiodotetrafluorobenzene (*p*-F₄DIB) with the halide salts of the benzyltrimethylammonium cation (NMe₃BzCl,

^a Department of Chemistry, Clemson University, 219 Hunter Laboratories, Clemson, SC 29634-0973, USA. E-mail: cmcmill@clemson.edu, billp@clemson.edu

^b Department of Chemistry, Furman University, Greenville, SC 29613, USA

† Dedicated to Professor Resnati, celebrating a career in fluorine and noncovalent chemistry on the occasion of his 70th birthday.



NMe₃BzBr, and NMe₃BzI) in a variety of solvents. *p*-F₄DIB is a widely used, strong halogen bond donor due to its electron-withdrawing fluorine substituents, while quaternary ammonium halide salts offer flexible anionic templates, lacking significant directional or numeric limitations at the halide anion, making them suitable for exploring structure-directing effects in cocrystal formation.^{30–33} The two-component system of (NMe₃BzX):(p-F₄DIB) can be equally interpreted as a three-component system of cation, anion, and organoiodine, or (NMe₃Bz⁺)(X⁻):(p-F₄DIB).

A search of the Cambridge Structural Database for cocrystals of *p*-F₄DIB reveals 729 hits, with 105 of these containing at least one ionic component. Common ionic components include pyridine-*N*-oxides,^{34–36} halides,^{37,38} and various ammonium-containing cations.^{39–41} Amongst the common organic solvents, solvates with methanol,^{37,38} ethanol,³⁸ dichloromethane,^{42,43} chloroform,³⁸ acetone,⁴⁴ acetonitrile,^{44–47} toluene⁴⁸ have been previously reported. For the salts NMe₃BzCl and NMe₃BzBr, unsolvated ionic cocrystals were more likely to be isolated, whereas the iodide salt provided primarily solvated ionic cocrystals of varying stoichiometry. The bromide and chloride-containing ionic cocrystals were often isostructural. Trends in void volume were analyzed using CCDC's *Mercury*⁴⁹ as well as the IUCr's *checkCIF*,^{50–52} revealing a significant chasm in the void volumes between the solvated and unsolvated structures.

Experimental

Synthesis of ionic cocrystals

Benzyltrimethylammonium chloride (purity 97%, CAS registry number 56-93-9), benzyltrimethylammonium bromide (purity 95+%, CAS registry number 5350-41-4), and 1,4-diiidotetrafluorobenzene (purity 97%, CAS registry number 392-57-4) were obtained from Oakwood Chemical. Benzyltrimethylammonium iodide (purity 95%, CAS registry number 4525-46-6) was obtained from Millipore Sigma. All

reagents and solvents were used as received. All ionic cocrystals were obtained *via* a 1:1 molar ratio reaction of the benzyltrimethylammonium halide salt and 1,4-diiidotetrafluorobenzene in the respective solvent under ambient conditions (Table 1). Many of the solvates had limited stability outside of the mother liquor, so no thermal analysis or powder X-ray diffraction studies were conducted. A representative synthesis is included.

Synthesis of NMe₃BzI:p-F₄DIB:EtOH. As a representative synthesis, benzyltrimethylammonium iodide (41 mg, 0.15 mmol) and 1,4-diiidotetrafluorobenzene (59 mg, 0.15 mmol) were combined with vigorous stirring in ca 10 mL of ethanol. Once dissolved, stirring was stopped, and the solvent was allowed to evaporate slowly under ambient conditions. Once crystal growth was observed, the vial was sealed to limit potential solvent loss or crystal decomposition. In most solvent systems, cocrystal formation was observed within seven days. Most of the solvated ionic cocrystals exhibited very limited stability outside of their mother liquor. Complete synthetic details for all twenty ionic cocrystals are provided in the SI.

X-ray crystallography. For single-crystal X-ray analysis, crystals were mounted on low-background cryogenic loops using paratone oil. Data were collected using Mo K α radiation ($\lambda = 0.71073 \text{ \AA}$) on a Bruker D8 Venture diffractometer with an Incoatec I μ s microfocus source and a Photon 2 detector or a Bruker D8 Quest diffractometer with a Photon 100 detector. Diffraction data were collected using φ and ω -scans and subsequently processed (SAINT) and scaled (SADABS) using the APEX3 software suite.⁵³ The structures were solved by intrinsic phasing (SHELXT) and refined by full-matrix least-squares techniques (SHELXL) on F^2 using the SHELXTL software suite.^{54,55}

All non-hydrogen atoms were refined anisotropically. As the acetonitrile molecules in 2(NMe₃BzCl):2(*p*-F₄DIB):MeCN, 2(NMe₃BzBr):2(*p*-F₄DIB):MeCN, and 4(NMe₃BzI):4(*p*-F₄DIB):MeCN lie on symmetry elements, they were constrained with a combination of DFIX, DANG, ISOR, and SIMU to achieve

Table 1 Ionic cocrystals obtained by NMe₃BzX salt and solvent

		NMe ₃ BzX salt		
		NMe ₃ BzCl	NMe ₃ BzBr	NMe ₃ BzI
Solvent	Methanol (MeOH)	NMe ₃ BzCl:p-F ₄ DIB	NMe ₃ BzBr:p-F ₄ DIB	NMe ₃ BzI:p-F ₄ DIB:MeOH 2(NMe ₃ BzI):3(<i>p</i> -F ₄ DIB)
	Ethanol (EtOH)	NMe ₃ BzCl:p-F ₄ DIB	3(NMe ₃ BzBr):4(<i>p</i> -F ₄ DIB)	NMe ₃ BzI:p-F ₄ DIB:EtOH
	<i>iso</i> -Propanol (<i>i</i> -PrOH)	NMe ₃ BzCl:p-F ₄ DIB	3(NMe ₃ BzBr):4(<i>p</i> -F ₄ DIB)	NMe ₃ BzI:p-F ₄ DIB: <i>i</i> -PrOH
	<i>Tert</i> -Butanol (<i>t</i> -BuOH)	NMe ₃ BzCl:p-F ₄ DIB	3(NMe ₃ BzBr):4(<i>p</i> -F ₄ DIB)	4(NMe ₃ BzI):5(<i>p</i> -F ₄ DIB)
	Acetonitrile (MeCN)	2(NMe ₃ BzCl):2(<i>p</i> -F ₄ DIB):MeCN	2(NMe ₃ BzBr):2(<i>p</i> -F ₄ DIB):MeCN	4(NMe ₃ BzI):4(<i>p</i> -F ₄ DIB):MeCN
	Acetone (Ace)	NMe ₃ BzCl:p-F ₄ DIB:Ace	NMe ₃ BzBr:p-F ₄ DIB:Ace	4(NMe ₃ BzI):4(<i>p</i> -F ₄ DIB):3(Ace)
	Dichloromethane (DCM)	NMe ₃ BzCl:p-F ₄ DIB	4(NMe ₃ BzBr):5(<i>p</i> -F ₄ DIB)	2(NMe ₃ BzI):2(<i>p</i> -F ₄ DIB):DCM
	Chloroform (CHCl ₃)	3(NMe ₃ BzCl):3(<i>p</i> -F ₄ DIB):2(CHCl ₃)	^a	2(NMe ₃ BzI):2(<i>p</i> -F ₄ DIB):CHCl ₃
	Iodomethane (CH ₃ I)	2(NMe ₃ BzI):2(<i>p</i> -F ₄ DIB):CH ₃ I ^b	2(NMe ₃ BzI):2(<i>p</i> -F ₄ DIB):CH ₃ I ^b	2(NMe ₃ BzI):2(<i>p</i> -F ₄ DIB):CH ₃ I
	Toluene	^c	^c	8(NMe ₃ BzI):3(<i>p</i> -F ₄ DIB)
	Ethylene glycol	NMe ₃ BzCl:p-F ₄ DIB	^c	4(NMe ₃ BzI):5(<i>p</i> -F ₄ DIB)

^a The crystal structure of the resulting crystals could not be reliably determined due to extensive twinning. ^b We note that *in situ* decomposition of the CH₃I solvent led to the formation of the solvated iodide salt cocrystal in all cases. ^c We observed recrystallization of the starting materials rather than formation of a cocrystal.



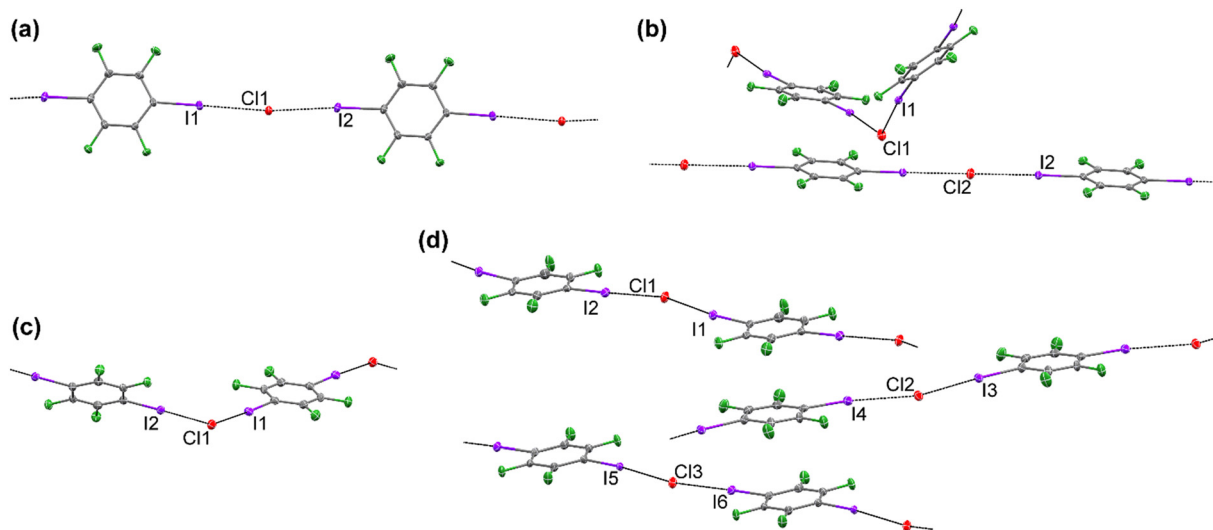


Fig. 1 Halogen bonding in $\text{NMe}_3\text{BzCl}:\text{p-F}_4\text{DIB}$ (a) (viewed down the c axis), $2(\text{NMe}_3\text{BzCl}):2(\text{p-F}_4\text{DIB}):\text{MeCN}$ (b) (viewed down the c^* axis), $\text{NMe}_3\text{BzCl}:\text{p-F}_4\text{DIB}:\text{Ace}$ (c) (viewed down the b axis), and $3(\text{NMe}_3\text{BzCl}):3(\text{p-F}_4\text{DIB}):2(\text{CHCl}_3)$ (d). Solvent molecules and hydrogen atoms are omitted for clarity. Atomic displacement ellipsoids are displayed at the 50% probability level. Carbon atoms are gray, fluorine atoms green, iodine atoms purple, chlorine atoms red, and bromine atoms brown.

chemically reasonable geometries. Two orientations of the ethanol molecule in $\text{NMe}_3\text{BzI}:\text{p-F}_4\text{DIB}:\text{EtOH}$ were modeled with reasonable SIMU constraints. Disorder within the acetone molecules of $4(\text{NMe}_3\text{BzI}):4(\text{p-F}_4\text{DIB}):3(\text{Ace})$ was constrained using reasonable SIMU constraints. The SI (Table S11) provides crystallographic data from the structure refinements.

Void calculations-methods

Solvent accessible void volumes were calculated using the crystal structure visualization and analysis software Mercury, designed by the Cambridge Crystallographic Data Centre (CCDC).⁴⁹ The pore analyzer tool was utilized to calculate the volumes of the void spaces with the solvents manually

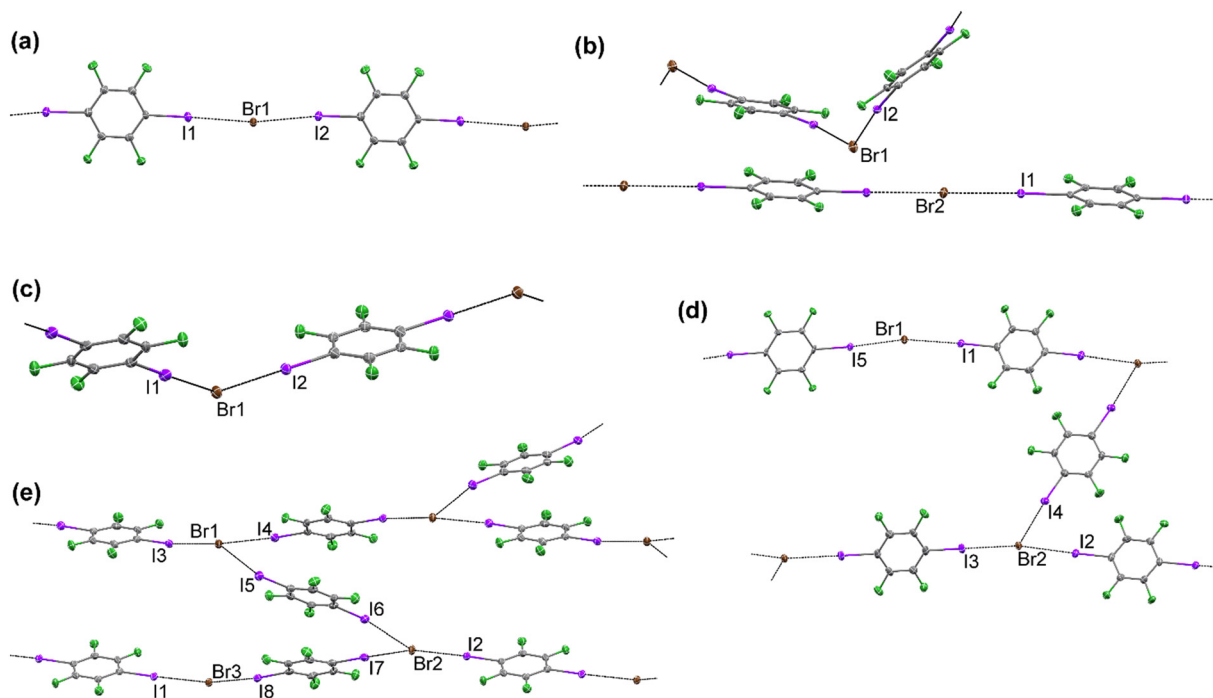


Fig. 2 Halogen bonding in $\text{NMe}_3\text{BzBr}:\text{p-F}_4\text{DIB}$ (a), $2(\text{NMe}_3\text{BzBr}):2(\text{p-F}_4\text{DIB}):\text{MeCN}$ (b), $\text{NMe}_3\text{BzBr}:\text{p-F}_4\text{DIB}:\text{Ace}$ (c), $4(\text{NMe}_3\text{BzBr}):5(\text{p-F}_4\text{DIB})$ (d), and $3(\text{NMe}_3\text{BzBr}):4(\text{p-F}_4\text{DIB})$ (e). Solvent molecules and hydrogen atoms are omitted for clarity. Atomic displacement ellipsoids are displayed at the 50% probability level.



alternating layers propagate in $[0\ 1\ 1]$ and $[0\ 1\ -1]$ directions. The combination of halogen bonding interactions in the 4:5 ionic cocrystal results in the formation of interpenetrating sheets, with a plane-to-plane angle of approximately 49° .

While the majority of solvents provided solvated ionic cocrystals when using NMe_3BzI , three unsolvated motifs were obtained: $4(\text{NMe}_3\text{BzI}):5(p\text{-F}_4\text{DIB})$, $8(\text{NMe}_3\text{BzI}):3(p\text{-F}_4\text{DIB})$, and $2(\text{NMe}_3\text{BzI}):3(p\text{-F}_4\text{DIB})$ (Fig. 3). The 4:5 ionic cocrystal is obtained when using ethylene glycol as the reaction solvent in the space group $P2_1/c$, just as in the $4(\text{NMe}_3\text{BzBr}):5(p\text{-F}_4\text{DIB})$ system. Once again, chains are interconnected by $p\text{-F}_4\text{DIB}$ molecules to form sheets. These interpenetrating sheets intersect at approximately 49° , matching the packing within the $4(\text{NMe}_3\text{BzBr}):5(p\text{-F}_4\text{DIB})$ system. The $8(\text{NMe}_3\text{BzI}):3(p\text{-F}_4\text{DIB})$ system crystallizes in the space group $P\bar{1}$ from toluene. In this case, in contrast to the extended halogen bonding motifs seen in the previously described systems, this ionic cocrystal contains three distinct, isolated halogen bonding units each consisting of one $p\text{-F}_4\text{DIB}$ molecule "capped" by two iodide anions through $\text{C-F}\cdots\text{I}$ halogen bonding. The remaining two iodide anions fill space within

the crystal lattice but are not involved in significant halogen bonding interactions. This is the only example in this study where long-range halogen bonding patterns were not observed. The final unsolvated, iodide-containing ionic cocrystal, $2(\text{NMe}_3\text{BzI}):3(p\text{-F}_4\text{DIB})$, was obtained from the same reaction that produced $\text{NMe}_3\text{BzI}:p\text{-F}_4\text{DIB}:\text{MeOH}$. The halogen bonding motif is similar to that of $4(\text{NMe}_3\text{BzBr}):5(p\text{-F}_4\text{DIB})$, with chains consisting of alternating $p\text{-F}_4\text{DIB}$ molecules and iodide anions, kinked at $45.228(6)^\circ$ and $35.548(6)^\circ$ about the two unique $\text{C-I}\cdots\text{I}\cdots\text{I-C}$ halogen bonds. The chains are linked into sheets *via* a $p\text{-F}_4\text{DIB}$ molecule, with an acute angle of $70.045(5)^\circ$ at the junction.

Solvated ionic cocrystals

When utilizing the chloride and bromide salts, acetonitrile, acetone, and chloroform yielded solvated ionic cocrystals. Both the chloride and bromide-containing cocrystals, $2(\text{NMe}_3\text{BzCl}):2(p\text{-F}_4\text{DIB}):\text{MeCN}$ and $2(\text{NMe}_3\text{BzBr}):2(p\text{-F}_4\text{DIB}):\text{MeCN}$ respectively (Fig. 1b and 2b), crystallize in the space group $C2/c$, with one fully unique NMe_3Bz^+ cation, two half

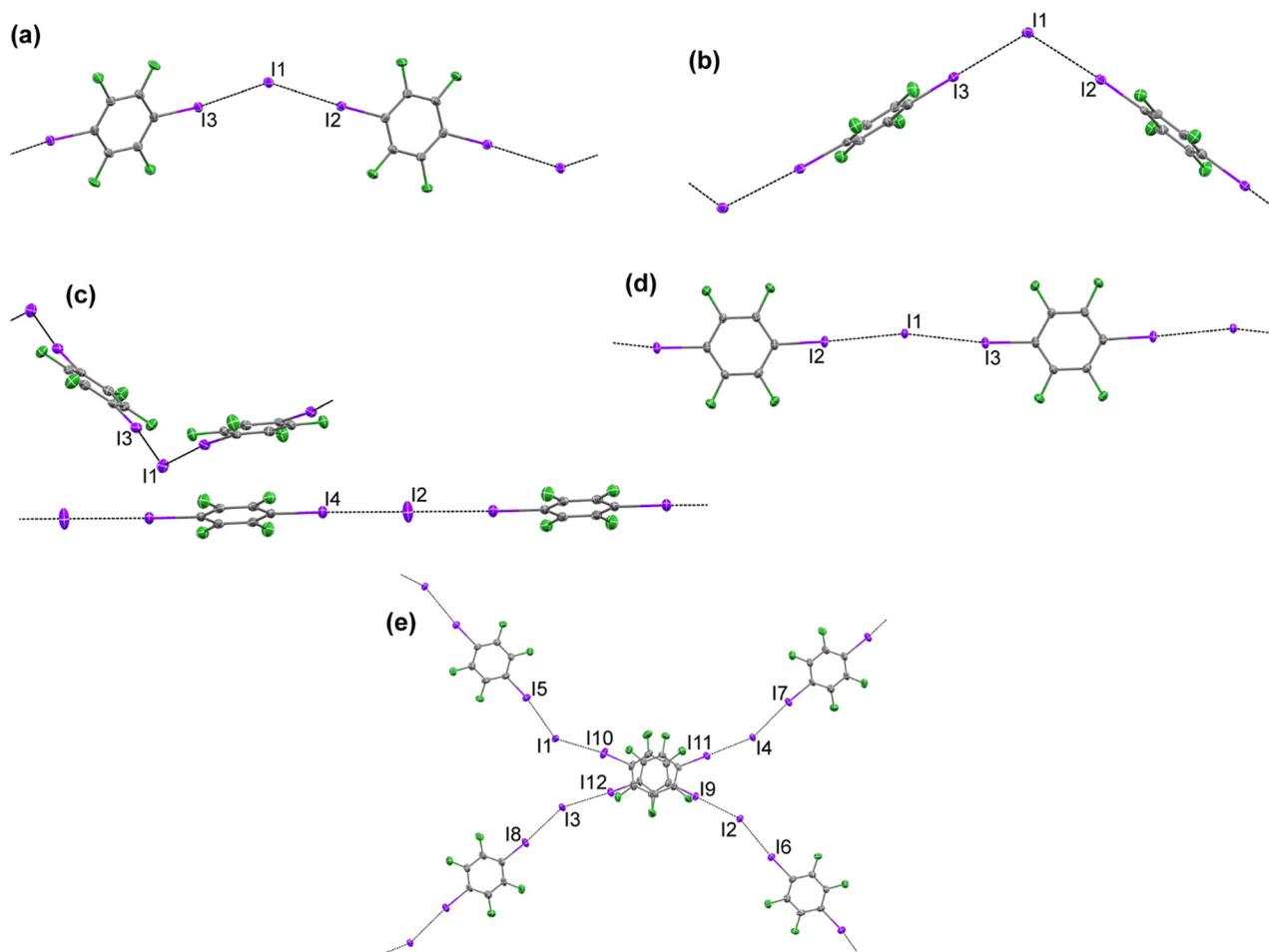


Fig. 4 Halogen bonding in $\text{NMe}_3\text{BzI}:p\text{-F}_4\text{DIB}:i\text{-PrOH}$ (a), $\text{NMe}_3\text{BzI}:p\text{-F}_4\text{DIB}:\text{MeOH}$ (b), $4(\text{NMe}_3\text{BzI}):4(p\text{-F}_4\text{DIB}):\text{MeCN}$ (c), $2(\text{NMe}_3\text{BzI}):2(p\text{-F}_4\text{DIB}):\text{CH}_3\text{I}$ (d), $4(\text{NMe}_3\text{BzI}):4(p\text{-F}_4\text{DIB}):3(\text{Ace})$ (e). Solvent molecules and hydrogen atoms are omitted for clarity. Atomic displacement ellipsoids are displayed at the 50% probability level.



in the same direction align in the *ac* plane, with the propagation direction varying for successive chains in different layers along the *b* axis.

When iodomethane was utilized as the crystallization solvent, $2(\text{NMe}_3\text{BzI}):2(p\text{-F}_4\text{DIB}):\text{CH}_3\text{I}$ was obtained regardless of which halide salt was used in the reaction (Fig. 4d). This is likely due to the formation of iodide anions during the decomposition of iodomethane, resulting in the preferential crystallization of iodide salts over their chloride or bromide analogs. The primary $\text{C}\cdots\text{I}\cdots\text{I}\cdots\text{I}\cdots\text{C}$ halogen bonding forms kinked chains ($\text{I}\cdots\text{I}\cdots\text{I}$ of $166.710(7)^\circ$). Chain propagation direction varies while moving along the *c* axis, from $[1\ 0\ 0]$ to $[1\ 1\ 0]$ to $[0\ 1\ 0]$.

The remaining solvated ionic cocrystals were obtained only in the $\text{NMe}_3\text{BzI}:p\text{-F}_4\text{DIB}$ system. These occurred in reactions with methanol, ethanol, isopropanol, dichloromethane, and chloroform. In the chloride and bromide systems, the alcohols and dichloromethane yielded only non-solvated ionic cocrystals. Chloroform yielded a 3:3:2 solvated ionic cocrystal when utilizing the chloride salt, differing from the 2:2:1 ratio of the iodide salt. The packing in the $\text{NMe}_3\text{BzI}:p\text{-F}_4\text{DIB}:\text{MeOH}$ (Fig. 4b) and $\text{NMe}_3\text{BzI}:p\text{-F}_4\text{DIB}:\text{EtOH}$ ionic cocrystals is quite similar, with only slight expansions in the orthorhombic cell parameters. In contrast, the $\text{NMe}_3\text{BzI}:p\text{-F}_4\text{DIB}:i\text{-PrOH}$ (Fig. 4a) ionic cocrystals are obtained in the space group $P\bar{1}$. Halogen bonding drives the formation of kinked chains in all three systems. The $\text{C}\cdots\text{I}\cdots\text{I}\cdots\text{I}\cdots\text{C}$ angle in the methanol and ethanol systems is similar, $109.466(18)^\circ$ and $112.58(1)^\circ$, respectively, whereas the chains in the *i*-PrOH system show less bending at $146.199(6)^\circ$. The $2(\text{NMe}_3\text{BzI}):2(p\text{-F}_4\text{DIB}):\text{DCM}$ ionic cocrystal obtained from dichloromethane shows a halogen bonding motif similar to the iodide-containing acetonitrile solvated ionic cocrystal (Fig. 4c), with both straight and kinked chain.. The $\text{C}\cdots\text{I}\cdots\text{I}\cdots\text{I}\cdots\text{C}$ angle of $136.554(14)^\circ$ is also similar to the acetonitrile system. Finally, the halogen bonding observed in the chloroform solvate $2(\text{NMe}_3\text{BzI}):2(p\text{-F}_4\text{DIB}):\text{CHCl}_3$ is analogous to that of the acetone-containing system (Fig. 4e), with chains in the *ac* plane alternating their propagation direction as they stack in the *b* direction.

Pore diameter comparison

An analysis of pore diameter, as calculated using CCDC's Mercury or IUCr's checkCIF tools after manual removal of the solvent molecule atoms, reveals several trends in the porosity of halogen-bonded ionic cocrystals (Table 2). As expected, solvent inclusion plays a dominant role in expanding accessible volume, with solvated ionic cocrystals exhibiting significantly higher helium-accessible volumes and maximum pore diameters than their solvent-free analogues. The identity of the halogen also influences porosity: iodine-based systems consistently show larger voids and wider pores than their bromine- or chlorine-containing counterparts, likely due to iodine's greater polarizability, larger size, and stronger, more directional halogen bonding (Fig. 5 and 6).

Higher donor-to-acceptor stoichiometries (e.g., 4:4 or 3:3) further enhance porosity, especially when paired with solvent inclusion, promoting the formation of more open and stable supramolecular frameworks. Unsurprisingly, a strong correlation is observed between maximum pore diameter and solvent-accessible void volume, though exceptions—such as the $4(\text{NMe}_3\text{BzI}):4(p\text{-F}_4\text{DIB}):3(\text{Ace})$ ionic cocrystal—highlight the limitations of automated void analysis. A significant jump in void volumes is observed between the solvated and unsolvated architectures, with approximately a 35% increase in maximum pore diameter between $4(\text{NMe}_3\text{BzI}):5(p\text{-F}_4\text{DIB})$, which has the largest pore diameter among the unsolvated

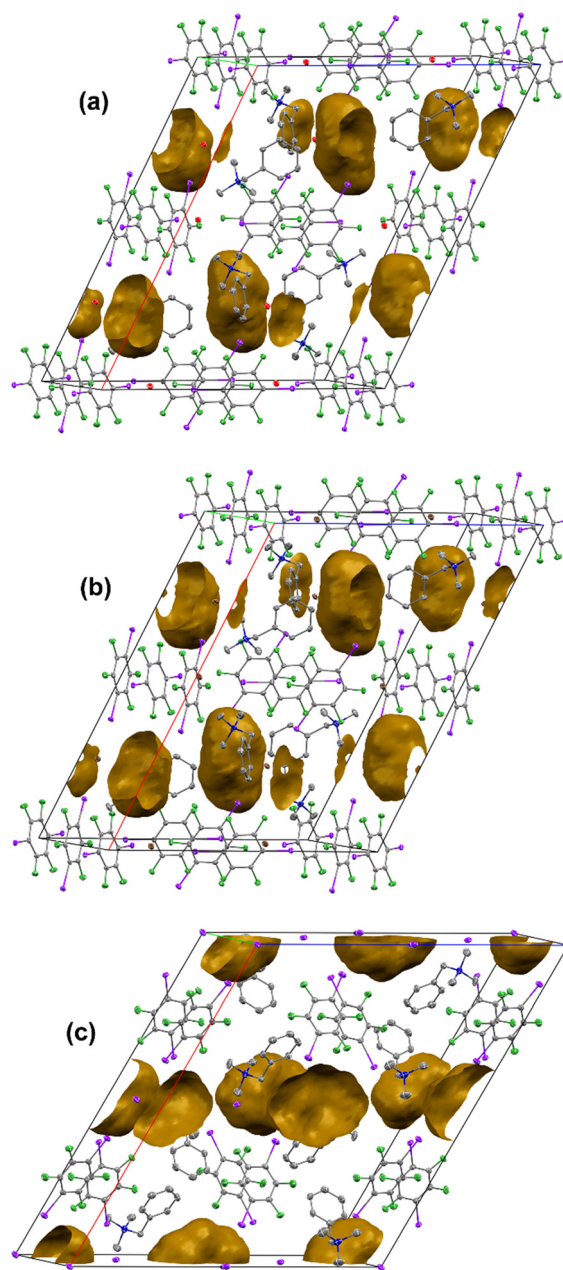


Fig. 5 Solvent voids in $2(\text{NMe}_3\text{BzI}):2(p\text{-F}_4\text{DIB}):\text{MeCN}$ (a), $2(\text{NMe}_3\text{BzBr}):2(p\text{-F}_4\text{DIB}):\text{MeCN}$ (b), and $4(\text{NMe}_3\text{BzI}):4(p\text{-F}_4\text{DIB}):\text{MeCN}$ (c).



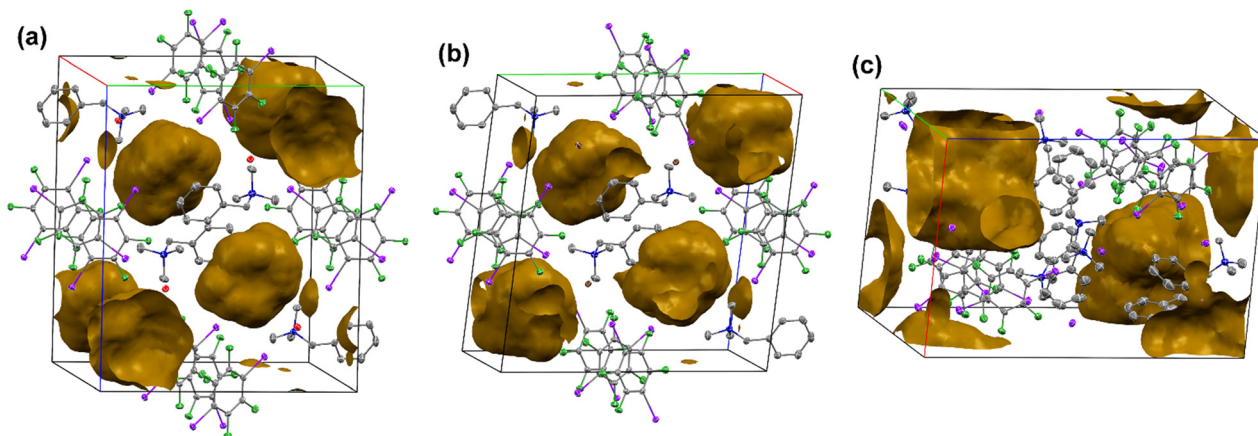


Fig. 6 Solvent voids in $\text{NMe}_3\text{BzCl}:p\text{-F}_4\text{DIB}:\text{Ace}$ (a), $\text{NMe}_3\text{BzBr}:p\text{-F}_4\text{DIB}:\text{Ace}$ (b), and $4(\text{NMe}_3\text{BzI}):4(p\text{-F}_4\text{DIB}):3(\text{Ace})$ (c). The a axis is red, the b axis is green, and the c axis is blue.

structures, and $4(\text{NMe}_3\text{BzI}):4(p\text{-F}_4\text{DIB}):\text{MeCN}$, which has the smallest pore diameter of the solvated structures. The Kitaigorodskii Packing Index (KPI), as calculated by the CALC VOID routine of PLATON, shows similar jumps. Within the

iodide salt-containing structures, there is a 5–10% decrease in the KPI when comparing solvated structures to their solvent-removed structures. Stable structures including the solvent contribution typically had KPI values of 65% of

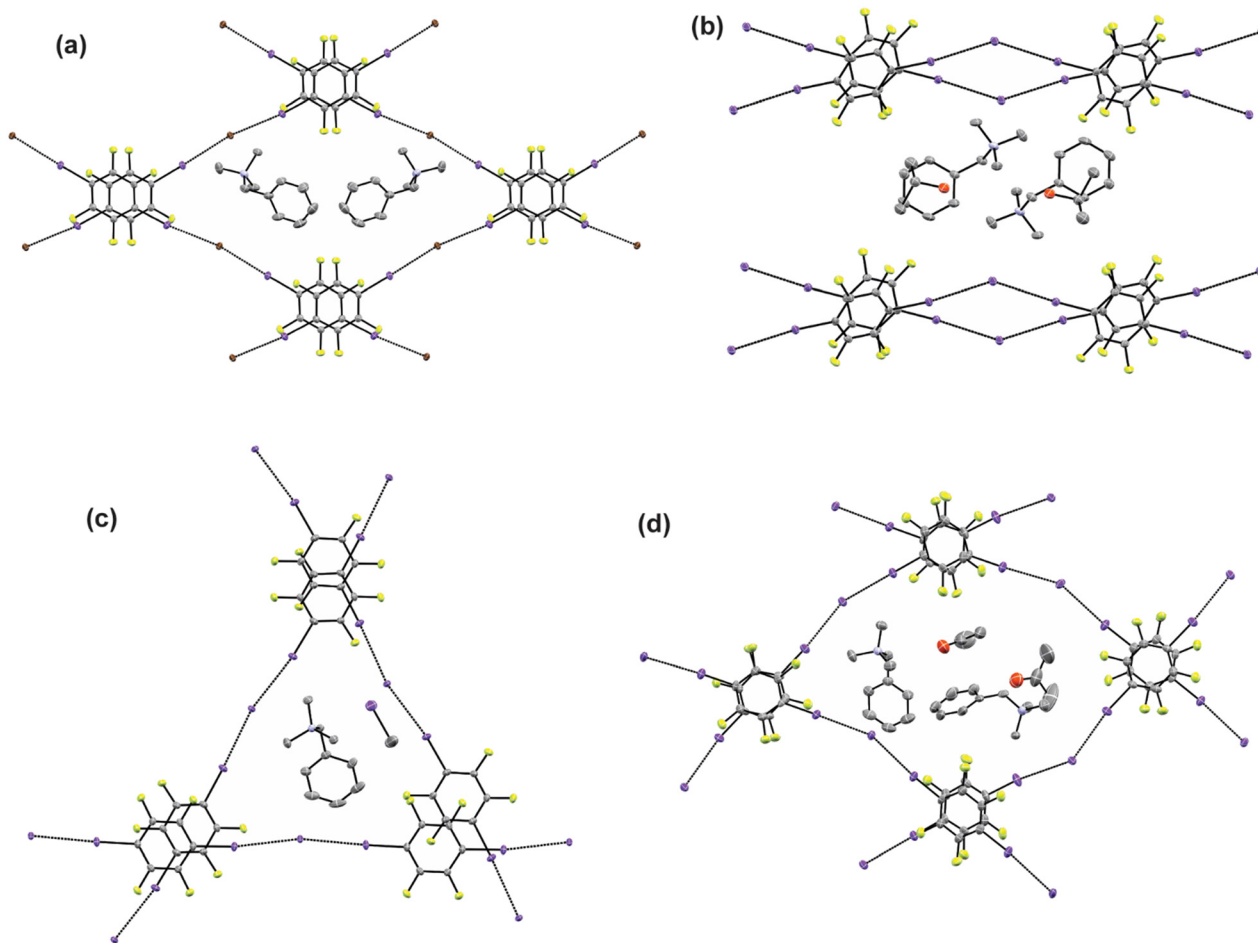


Fig. 7 Solvent and cation containing channels formed in $\text{NMe}_3\text{BzBr}:p\text{-F}_4\text{DIB}$ (a), $\text{NMe}_3\text{BzI}:p\text{-F}_4\text{DIB}:i\text{-PrOH}$ (b), $\text{NMe}_3\text{BzI}:p\text{-F}_4\text{DIB}:\text{CH}_3\text{I}$ (c), and $4(\text{NMe}_3\text{BzI}):4(p\text{-F}_4\text{DIB}):3(\text{Ace})$ (d). Hydrogen atoms are omitted for clarity. Atomic displacement ellipsoids are displayed at the 50% probability level.



higher, whereas manually removing the solvent molecules and recalculating the KPI shows values between 57% and 65%. This compares favorably to the stable lattices formed by unsolvated ionic cocrystals, showing KPI values greater than 62%.

Packing scope and limitations of 1 : 1 ionic cocrystals of NMe₃BzX-*p*-F₄DIB and their solvates

It is apparent from the void analysis above that equimolar ionic cocrystal ratios of NMe₃BzI-*p*-F₄DIB adopt packing arrangements with significant void space that is ultimately occupied by solvent molecules. Given the variation in structure types observed in this series of structures (Table S11) it seems the 1:1 iodide lattice is particularly flexible to accommodate the diversity of solvents studied here. Several packing themes were observed. In the 1:1 unsolvated systems NMe₃BzCl-*p*-F₄DIB and NMe₃BzBr-*p*-F₄DIB (Fig. 7a), a similar rhomboidal channel contained the ammonium component. A frequent arrangement obtained in the iodide-containing, solvated systems was the consolidation of the solvent and ammonium molecules between sheets of the halogen containing components, exemplified by NMe₃BzI-*p*-F₄DIB-*i*-PrOH (Fig. 7b). The ionic cocrystal obtained from iodomethane displays a trigonal channel (Fig. 7c). Finally, the ionic cocrystal obtained from acetone shows a more distorted rhomboidal channel hosting the solvent molecules and ammonium cations (Fig. 7d). In all cases, the alignment of chains also serves to localize the fluorinated portion of the structure throughout the lattice.

Conclusions

The reaction of the common halogen bond donor 1,4-diiodotetrafluorobenzene (*p*-F₄DIB) with the halide salts of the trimethylbenzyl ammonium cation (NMe₃BzX, X = Cl, Br, I) in a wide variety of organic solvents revealed a strong correlation between the identity of the halide anion and the resulting solid-state structure. When utilizing NMe₃BzI, a strong preference for solvated structures was observed, with eight solvated and three unsolvated motifs observed across 11 solvents. The unsolvated structures were obtained with the unequal NMe₃BzI to *p*-F₄DIB ratios 2:3, 8:3, and 4:5. In contrast, the solvated structures were all obtained in equal halogen bond acceptor:donor ratios, with NMe₃BzI-*p*-F₄DIB:solvent ratios of 1:1:1, 2:2:1, and 4:4:1. The preference for solvation in the solid state is reversed when moving to the NMe₃BzBr and NMe₃BzCl systems, with the majority of the structures obtained being free from solvent inclusion. Across seven solvents in the NMe₃BzBr system (excluding iodomethane), five unsolvated structures, in 1:1, 3:4, and 4:5 acceptor:donor ratios, and two solvated structures, in 1:1:1 and 2:2:1 acceptor:donor:solvent ratios, were obtained. When moving to NMe₃BzCl, the preference for unsolvated structures continues, with six different solvents providing the same 1:1 NMe₃BzCl-*p*-F₄DIB structure. Three other solvated structures were obtained in 1:1:1, 2:2:2,

and 3:3:2 ratios. The crystal packing and halogen bonding motifs were identical, except for the slight size difference of the halogen anion, in bromide- and chloride-containing crystals of the same ratios. In the iodides we observe two instances where the ionic cocrystal ratio approaches 1:1 (in the 2:3 ionic cocrystal and the 4:5 ionic cocrystal) that form sufficiently condensed packing lattices without solvent incorporation. But in a true equimolar ratio of NMe₃BzI-*p*-F₄DIB, we have not yet observed packing that is entirely supported by solvent-free halogen bonding. These results highlight the versatility of halogen bonding to accommodate a variety of packing motifs, as well as its sensitivity to reaction conditions.

Author contributions

The manuscript was written through the contributions of all authors. All authors have given approval to the final version of the manuscript.

Conflicts of interest

There are no conflicts to declare.

Data availability

Supplementary information (SI): For ESI and crystallographic data in CIF or other electronic format. See DOI: <https://doi.org/10.1039/d5ce00832h>.

CCDC 2477133–2477141, 2477245, 2477246 and 2477290–2477298 contain the supplementary crystallographic data for this paper.^{59a–t}

Acknowledgements

AJP acknowledges the United States Air Force Institute of Technology Civilian Institutions for fellowship support.

References

- G. Cavallo, P. Metrangolo, R. Milani, T. Pilati, A. Priimagi, G. Resnati and G. Terraneo, *Chem. Rev.*, 2016, **116**, 2478–2601.
- G. R. Desiraju, P. Shing Ho, L. Kloo, A. C. Legon, R. Marquardt, P. Metrangolo, P. Politzer, G. Resnati and K. Rissanen, *Pure Appl. Chem.*, 2013, **85**, 1711–1713.
- N. Baus Topić, N. Bedeković, K. Lisac, V. Stilinović and D. Cinčić, *Cryst. Growth Des.*, 2022, **22**, 3981–3989.
- L. H. E. Wieske and M. Erdélyi, *J. Am. Chem. Soc.*, 2024, **146**, 3–18.
- M. Erdélyi, C. Esterhuysen and W. Zhu, *Chem*, 2021, **86**, 1229–1230.
- S. An, A. Hao and P. Xing, *ACS Nano*, 2022, **16**, 19220–19228.
- B. Topaloğlu Aksoy, B. Dedeoglu, Y. Zorlu, M. M. Ayhan and B. Çoşut, *CrystEngComm*, 2022, **24**, 5630–5641.
- E. Nieland, D. Komisarek, S. Hohloch, K. Wurst, V. Vasylyeva, O. Weingart and B. M. Schmidt, *Chem. Commun.*, 2022, **58**, 5233–5236.



- 9 P. Politzer, J. S. Murray and T. Clark, *Phys. Chem. Chem. Phys.*, 2013, **15**, 11178–11189.
- 10 L. C. Gilday, S. W. Robinson, T. A. Barendt, M. J. Langton, B. R. Mullaney and P. D. Beer, *Chem. Rev.*, 2015, **115**, 7118–7195.
- 11 D. M. Ivanov, N. A. Bokach, V. Yu. Kukushkin and A. Frontera, *Chem. – Eur. J.*, 2022, **28**, 1–12.
- 12 P. Metrangolo, F. Meyer, T. Pilati, G. Resnati and G. Terraneo, *Angew. Chem., Int. Ed.*, 2008, **47**, 6114–6127.
- 13 (a) P. Metrangolo, F. Meyer, T. Pilati, G. Resnati and G. Terraneo, *Chem. – Eur. J.*, 2001, **7**, 2511–2519.
- 14 J. Xu, X. Liu, T. Lin, J. Huang and C. He, *Macromolecules*, 2005, **38**, 3554–3557.
- 15 P. Metrangolo, C. Präsang, G. Resnati, R. Liantonio, A. C. Whitwood and D. W. Bruce, *Chem. Commun.*, 2006, 3290–3292.
- 16 J. Xu, X. Liu, J. K. P. Ng, T. Lin and C. He, *J. Mater. Chem.*, 2006, **16**, 3540–3545.
- 17 M. H. Kolář and O. Tabarrini, *J. Med. Chem.*, 2017, **60**, 8681–8690.
- 18 L. Mendez, G. Henriquez, S. Sirimulla and M. Narayan, *Molecules*, 2017, **22**, 1–15.
- 19 A. J. Cruz-Cabeza, S. Karki, L. Fábrián, T. Friić, G. M. Day and W. Jones, *Chem. Commun.*, 2010, **46**, 2224–2226.
- 20 S. Cherukuvada and A. Nangia, *Chem. Commun.*, 2014, **50**, 906–923.
- 21 A. M. Healy, Z. A. Worku, D. Kumar and A. M. Madi, *Adv. Drug Delivery Rev.*, 2017, **117**, 25–46.
- 22 S. J. Dalgarno, P. K. Thallapally, J. Tian and J. L. Atwood, *New J. Chem.*, 2008, **32**, 2095–2099.
- 23 D. Giron, *J. Therm. Anal. Calorim.*, 2001, 37–60.
- 24 A. Nangia, *Cryst. Growth Des.*, 2006, **6**, 2–4.
- 25 D. Braga, F. Grepioni, L. Maini and M. Polito, in *Molecular Networks (Structure and Bonding)*, ed. M. W. Hosseini, Springer, 2009, vol. 132, pp. 25–50.
- 26 G. P. Stahly, *Cryst. Growth Des.*, 2007, **7**, 1007–1026.
- 27 L. Turunen, F. Pan, N. K. Beyeh, M. Cetina, J. F. Trant, R. H. A. Ras and K. Rissanen, *CrystEngComm*, 2017, **19**, 5223–5229.
- 28 Y. Vasilopoulos, J. Heyda, J. Rohlíček, E. Škořepová, V. Zvoniček and M. Šoóš, *J. Phys. Chem. B*, 2022, **126**, 503–512.
- 29 A. Mukherjee, S. Tothadi and G. R. Desiraju, *Acc. Chem. Res.*, 2014, **47**, 2514–2524.
- 30 H. T. Le and A. Goto, *Cell Rep. Phys. Sci.*, 2021, **2**, 1–21.
- 31 N. B. Topić, E. Topić, L. Fotović and V. Stilinović, *Cryst. Growth Des.*, 2024, **24**, 1214–1226.
- 32 L. Posavec, V. Nemeč, V. Stilinović and D. Cinčić, *Cryst. Growth Des.*, 2021, **21**, 6044–6050.
- 33 C. Loy, M. Zeller and S. V. Rosokha, *Crystals*, 2020, **10**, 1–14.
- 34 P. V. Petunin, E. V. Tretyakov, M. K. Shurikov, D. E. Votkina, G. V. Romanenko, A. A. Dmitriev, N. P. Gritsan, D. M. Ivanov, R. M. Gomila, A. Frontera, G. Resnati, V. Y. Kukushkin and P. S. Postnikov, *Cryst. Growth Des.*, 2024, **24**, 2104–2116.
- 35 R. Liu, H. Wang and W. J. Jin, *Cryst. Growth Des.*, 2017, **17**, 3331–3337.
- 36 J. M. Rautiainen, A. Valkonen, J. Lundell, K. Rissanen and R. Puttreddy, *Adv. Sci.*, 2024, **11**, 1–12.
- 37 K. Lisac and D. Cinčić, *Crystals*, 2017, **7**, 1–11.
- 38 K. Raatikainen and K. Rissanen, *Cryst. Growth Des.*, 2010, **10**, 3638–3646.
- 39 K. Kobra, S. O'Donnell, A. Ferrari, C. D. McMillen and W. T. Pennington, *New J. Chem.*, 2018, **42**, 10518–10528.
- 40 M. C. Pfrunder, A. S. Micallef, L. Rintoul, D. P. Arnold, K. J. P. Davy and J. McMurtrie, *Cryst. Growth Des.*, 2014, **14**, 6041–6047.
- 41 J. Viger-Gravel, I. Korobkov and D. L. Bryce, *Cryst. Growth Des.*, 2011, **11**, 4984–4995.
- 42 A. S. Mikherdov, M. Jin and H. Ito, *Chem. Sci.*, 2023, **14**, 4485–4494.
- 43 X. Ding, M. Tuikka and M. Haukka, *Crystals*, 2020, **10**, 1–12.
- 44 L. Posavec and D. Cinčić, *Cryst. Growth Des.*, 2024, **24**, 7514–7523.
- 45 Y. N. Toikka, G. L. Starova, V. V. Suslonov, R. M. Gomila, A. Frontera, V. Y. Kukushkin and N. A. Bokach, *Cryst. Growth Des.*, 2023, **23**, 5194–5203.
- 46 H. M. Tang, Z. Y. Quan, B. Ding, X. G. Wang, B. Tang, Z. G. Huang and E. C. Yang, *Cryst. Growth Des.*, 2024, **24**, 5211–5221.
- 47 L. Happonen, J. M. Rautiainen and A. Valkonen, *Cryst. Growth Des.*, 2021, **21**, 3409–3419.
- 48 S. Shankar, O. Chovnik, L. J. W. Shimon, M. Lahav and M. E. Van Der Boom, *Cryst. Growth Des.*, 2018, **18**, 1967–1977.
- 49 C. F. MacRae, I. Sovago, S. J. Cottrell, P. T. A. Galek, P. McCabe, E. Pidcock, M. Platings, G. P. Shields, J. S. Stevens, M. Towler and P. A. Wood, *J. Appl. Crystallogr.*, 2020, **53**, 226–235.
- 50 A. L. Spek, *Inorg. Chim. Acta*, 2018, **470**, 232–237.
- 51 A. L. Spek, *J. Appl. Crystallogr.*, 2003, **36**, 7–13.
- 52 A. L. Spek, *Acta Crystallogr., Sect. D: Biol. Crystallogr.*, 2009, **65**, 148–155.
- 53 Bruker, *Bruker AXS*, 2017.
- 54 G. M. Sheldrick, *Acta Crystallogr., Sect. C: Struct. Chem.*, 2015, **71**, 3–8.
- 55 O. V. Dolomanov, L. J. Bourhis, R. J. Gildea, J. A. K. Howard and H. Puschmann, *J. Appl. Crystallogr.*, 2009, **42**, 339–341.
- 56 A. L. Spek, *J. Appl. Crystallogr.*, 2003, **36**, 7–13.
- 57 L. Brammer, E. A. Bruton and P. Sherwood, *Cryst. Growth Des.*, 2001, **1**, 277–290.
- 58 J. P. M. Lommerse, A. J. Stone, R. Taylor and F. H. Allen, *J. Am. Chem. Soc.*, 1996, **118**, 3108–3116.
- 59 (a) CCDC 2477133: Experimental Crystal Structure Determination, 2025, DOI: [10.5517/ccdc.csd.cc2p4nj1](https://doi.org/10.5517/ccdc.csd.cc2p4nj1); (b) CCDC 2477134: Experimental Crystal Structure Determination, 2025, DOI: [10.5517/ccdc.csd.cc2p4nk2](https://doi.org/10.5517/ccdc.csd.cc2p4nk2); (c) CCDC 2477135: Experimental Crystal Structure Determination, 2025, DOI: [10.5517/ccdc.csd.cc2p4nl3](https://doi.org/10.5517/ccdc.csd.cc2p4nl3); (d) CCDC 2477136: Experimental Crystal Structure Determination, 2025, DOI: [10.5517/ccdc.csd.cc2p4nm4](https://doi.org/10.5517/ccdc.csd.cc2p4nm4); (e) CCDC 2477137: Experimental Crystal Structure Determination, 2025, DOI: [10.5517/ccdc.csd.cc2p4nn5](https://doi.org/10.5517/ccdc.csd.cc2p4nn5); (f)



- CCDC 2477138: Experimental Crystal Structure Determination, 2025, DOI: [10.5517/ccdc.csd.cc2p4np6](https://doi.org/10.5517/ccdc.csd.cc2p4np6); (*g*)
- CCDC 2477139: Experimental Crystal Structure Determination, 2025, DOI: [10.5517/ccdc.csd.cc2p4nq7](https://doi.org/10.5517/ccdc.csd.cc2p4nq7); (*h*)
- CCDC 2477140: Experimental Crystal Structure Determination, 2025, DOI: [10.5517/ccdc.csd.cc2p4nr8](https://doi.org/10.5517/ccdc.csd.cc2p4nr8); (*i*)
- CCDC 2477141: Experimental Crystal Structure Determination, 2025, DOI: [10.5517/ccdc.csd.cc2p4ns9](https://doi.org/10.5517/ccdc.csd.cc2p4ns9); (*j*)
- CCDC 2477245: Experimental Crystal Structure Determination, 2025, DOI: [10.5517/ccdc.csd.cc2p4s4s](https://doi.org/10.5517/ccdc.csd.cc2p4s4s); (*k*)
- CCDC 2477246: Experimental Crystal Structure Determination, 2025, DOI: [10.5517/ccdc.csd.cc2p4s5t](https://doi.org/10.5517/ccdc.csd.cc2p4s5t); (*l*)
- CCDC 2477290: Experimental Crystal Structure Determination, 2025, DOI: [10.5517/ccdc.csd.cc2p4tl8](https://doi.org/10.5517/ccdc.csd.cc2p4tl8); (*m*)
- CCDC 2477291: Experimental Crystal Structure Determination, 2025, DOI: [10.5517/ccdc.csd.cc2p4tm9](https://doi.org/10.5517/ccdc.csd.cc2p4tm9); (*n*)
- CCDC 2477292: Experimental Crystal Structure Determination, 2025, DOI: [10.5517/ccdc.csd.cc2p4tnb](https://doi.org/10.5517/ccdc.csd.cc2p4tnb); (*o*)
- CCDC 2477293: Experimental Crystal Structure Determination, 2025, DOI: [10.5517/ccdc.csd.cc2p4tpc](https://doi.org/10.5517/ccdc.csd.cc2p4tpc); (*p*)
- CCDC 2477294: Experimental Crystal Structure Determination, 2025, DOI: [10.5517/ccdc.csd.cc2p4tqd](https://doi.org/10.5517/ccdc.csd.cc2p4tqd); (*q*)
- CCDC 2477295: Experimental Crystal Structure Determination, 2025, DOI: [10.5517/ccdc.csd.cc2p4trf](https://doi.org/10.5517/ccdc.csd.cc2p4trf); (*r*)
- CCDC 2477296: Experimental Crystal Structure Determination, 2025, DOI: [10.5517/ccdc.csd.cc2p4tsg](https://doi.org/10.5517/ccdc.csd.cc2p4tsg); (*s*)
- CCDC 2477297: Experimental Crystal Structure Determination, 2025, DOI: [10.5517/ccdc.csd.cc2p4tth](https://doi.org/10.5517/ccdc.csd.cc2p4tth); (*t*)
- CCDC 2477298: Experimental Crystal Structure Determination, 2025, DOI: [10.5517/ccdc.csd.cc2p4tvj](https://doi.org/10.5517/ccdc.csd.cc2p4tvj).

